THE JOURNAL OF PHYSICAL CHEMISTRY LETTERS
A JOURNAL OF THE AMERICAN CHEMICAL SOCIETY

pubs.acs.org/JPCL

Letter

Regularized and Opposite Spin-Scaled Functionals from Møller–Plesset Adiabatic Connection—Higher Accuracy at Lower Cost

Kimberly J. Daas, Derk P. Kooi, Nina C. Peters, Eduardo Fabiano, Fabio Della Sala, Paola Gori-Giorgi, and Stefan Vuckovic*

Cite This: *J. Phys. Chem. Lett.* 2023, 14, 8448–8459

Read Online

ACCESS | Metrics & More | Article Recommendations | Supporting Information

ABSTRACT: Noncovalent interactions (NCIs) play a crucial role in biology, chemistry, material science, and everything in between. To improve pure quantum-chemical simulations of NCIs, we propose a methodology for constructing approximate correlation energies by combining an interpolation along the Møller–Plesset adiabatic connection (MP AC) with a regularization and spin-scaling strategy applied to MP2 correlation energies. This combination yields $c_{os}\kappa_{os}$-SPL2, which exhibits superior accuracy for NCIs compared to any of the individual strategies. With the N^4 formal scaling, $c_{os}\kappa_{os}$-SPL2 is competitive or often outperforms more expensive dispersion-corrected double hybrids for NCIs. The accuracy of $c_{os}\kappa_{os}$-SPL2 particularly shines for anionic halogen bonded complexes, where it surpasses standard dispersion-corrected DFT by a factor of 3 to 5.

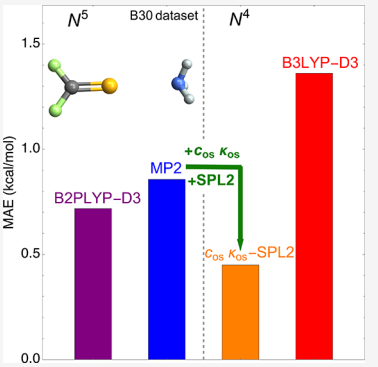

Noncovalant interactions (NCIs) play a crucial role in a variety of fields including biology, chemistry, material science, and everything in between.[1−13] Second order Møller–Plesset perturbation theory (MP2) has been used extensively to study NCIs[2,14] because it includes dispersion interactions and also has more favorable scalings compared to other wave function methods such as CCSD(T). However, MP2 does have its downsides, because it is known to fail for $\pi-\pi$ stacking complexes and generally for NCIs involving highly polarizable molecules.[15] More recently, it has been observed that MP2 and even the whole MP series have increasingly large errors for large complexes,[16] restricting the chemical space of NCIs that MP2 can be meaningfully applied to. Multiple methods have been introduced to increase the accuracy of MP2 by manipulating the underlying MP2 equations,[15,17−20] such as spin-component-scaled (SCS) MP2,[17] and spin-opposite-scaled (SOS) MP2.[18] SOS-MP2 does not only often improve the accuracy of MP2, but is also cheaper (scales formally as N^4) than the original MP2 (N^5). Another way to improve MP2 energies is to prevent their divergence when the HOMO–LUMO orbital gap closes through regularization,[15,20] and to mix MP2 with density functional theory (DFT) as in double hybrids (e.g., B2PLYP).[21−26] However, (with some exceptions[23−25]), when there is no dispersion correction, double hybrids typically worsen MP2 for NCIs.[10,21,22,27−29]

In our previous work,[30] we introduced a new class of functionals that directly approximate the Møller–Plesset adiabatic connection (AC),[31,32] which is the AC that gives an exact expression for the quantum-chemical correlation energy and has the MP series as weak coupling Taylor expansion. The idea behind these functionals is that by adding information for the large coupling limit, we can introduce a curvature in the underlying AC curve that is completely missed by MP2.[33] This curvature has been shown to play a very important role in describing NCIs, particularly as the ratio between dispersion and electrostatics in NCIs grows.[33] Our MP AC approach is fundamentally different from double hybrids, which rely on error cancellations between exact exchange and MP2 and their approximate semilocal counterparts. Instead, our MP AC approach uses the exact information from the weak coupling limit of MP AC—the full amounts of both exact exchange and MP2. One then recovers correlation energy with MP AC, by performing an interpolation between its weak- and strong-coupling limits. The resulting functionals based on this interpolation strategy either provide major improvements or are on par with dispersion-enhanced (double) hybrids and massively improve over MP2, particularly for large, $\pi-\pi$-stacking, and charge-transfer complexes.[30] The MP AC interpolation approach introduces a negligible additional cost to MP2 calculations, and because of that, it can

Received: July 4, 2023
Accepted: September 5, 2023
Published: September 18, 2023

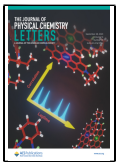

also be viewed as a zero-cost correction to MP2 correlation energies. Consequently, the computational cost of current MP AC functionals is the same as that of double hybrids. Nevertheless, their N^5 formal scaling can be prohibitive for large complexes, especially compared to the more feasible N^4 formal scaling of standard DFT hybrids.

In this work, we demonstrate the robustness of our MP AC functionals by applying them to different variants of MP2 and show how their cost and accuracy can be improved simultaneously. Utilizing this corrective power, we combine the MP AC approach to only the spin-opposite part of MP2 and the regularized version thereof, yielding massive improvements over SOS-MP2 for NCIs. This scaling-lowering strategy[18] ($N^5 \rightarrow N^4$) not only retains the accuracy of the original MP AC approach that uses "bare" MP2, but also gives major improvements across various classes of NCIs.

Figure 1 demonstrates the corrective power of a successful MP AC interpolation form, called SPL2,[30] i.e., containing two

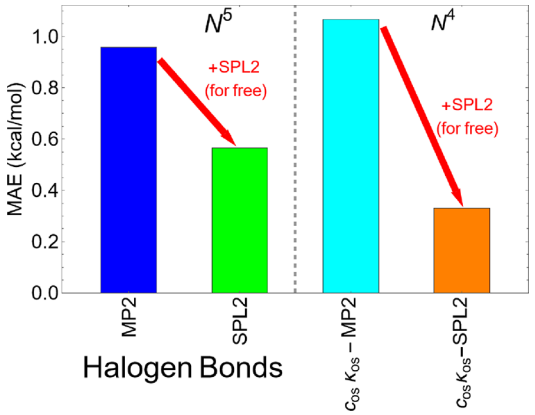

Figure 1. MAE (Mean Absolute Error) of MP2, SPL2, $c_{os}\kappa_{os}$-MP2, and $c_{os}\kappa_{os}$-SPL2 for the halogen bonded complexes of B30[34] and X40[35] (see Figure 7 for more detail on the complexes and Table 1 for individual methods).

terms of the Seidl, Perdew, and Levy (SPL)[36] interpolation formula. The individual bars show the mean absolute errors (MAE) for the interaction energies of halogen-bonded complexes. When "bare" MP2 (blue) is applied to these complexes, we get an MAE of slightly less than 1 kcal/mol. Applying SPL2 (the red arrow) to it, the error reduced to less than 0.6 kcal/mol. This is a substantial change relative to the magnitude of the interaction energies of halogen-bonded complexes. Now we consider a cost-lowering strategy and we take only the spin-opposite part of it, rescale it, and apply to it a specific regularization[15,20] to obtain $c_{os}\kappa_{os}$-MP2, which will be described in detail in the following. Once we go from MP2 (blue; N^5 scaling) to (light blue; N^4 scaling), the MAE increases slightly. However, SPL2 corrects $c_{os}\kappa_{os}$-MP2 to yield $c_{os}\kappa_{os}$-SPL2 (orange), which gives now improved results (MAE less than 0.4 kcal/mol) even with the more expensive and original SPL2 method (green). At this point, we should remember that both of the red arrows in Figure 1 practically come at no additional cost to the original MP2 calculations, be it MP2 or $c_{os}\kappa_{os}$-MP2. In what follows, we will detail the theoretical foundation for the construction of our methods.

Constructing MP AC. The Møller–Plesset adiabatic connection (MP AC) connects the (noninteracting) Hartree–Fock (HF) system to the physical system through the following Hamiltonian,[32,37−39]

$$\hat{H}_\lambda = \hat{T} + \hat{V}_{\text{ext}} + \lambda\hat{V}_{ee} + (1-\lambda)(\hat{J} + \hat{K}) \tag{1}$$

with $\lambda \geq 0$ the coupling constant, $\hat{T}$ the kinetic energy, $\hat{V}_{ee}$ the electron repulsion operator, $\hat{V}_{\text{ext}}$ representing the external potential, and $\hat{J} = \hat{J}[\rho^{\text{HF}}]$ and $\hat{K} = \hat{K}[\{\phi_i^{\text{HF}}\}]$ being the standard HF Coulomb and exchange operators. The last two are functionals of the HF density, ρ^{HF}, and the occupied orbitals, ϕ_i^{HF}, and are λ-independent. The correlation energy (exact energy minus HF energy) can be obtained by applying the Hellman–Feynman theorem to eq 1,[16,30,32,37−40]

$$E_c = \int_0^1 W_{c,\lambda}\mathrm{d}\lambda \tag{2}$$

where $W_{c,\lambda}$ is the AC integrand,

$$W_{c,\lambda} = \langle\Psi_\lambda|\hat{V}_{ee} - \hat{J} - \hat{K}|\Psi_\lambda\rangle - \langle\Psi_0|\hat{V}_{ee} - \hat{J} - \hat{K}|\Psi_0\rangle \tag{3}$$

with Ψ_λ being the wave function that minimizes $\hat{H}_\lambda$. The small-λ expansion of $W_{c,\lambda}$ is then the standard MP series,

$$W_{c,\lambda\rightarrow 0} = \sum_{n=2}^{\infty} nE_c^{\text{MP}n}\lambda^{n-1} \tag{4}$$

The large λ expansion of the MP AC has the form[32,38]

$$W_{c,\lambda\rightarrow\infty} = W_{c,\infty} + \frac{W_{1/2}}{\sqrt{\lambda}} + \frac{W_{3/4}}{\lambda^{3/4}} + \ldots \tag{5}$$

with

$$W_{c,\infty} = E_{el}[\rho^{\text{HF}}] + E_x \tag{6}$$

where $E_{el}[\rho]$ is[32,38] the classical electrostatic energy of N point charges bound by a charge density $\rho(\mathbf{r})$ of opposite sign, with $\int\rho(\mathbf{r})\mathrm{d}\mathbf{r} = N$. While gradient expansion approximations have recently been introduced for both E_{el} and $W_{1/2}$,[39] here we will approximate $W_{c,\infty}$ from the following inequality,

$$W_{c,\infty} \leq W_\infty^{\text{DFT}} + E_x \tag{7}$$

This inequality links $W_{c,\infty}$ to W_∞^{DFT} from the strong coupling limit of the DFT density-fixed AC.[41−46] In our previous work,[30] we introduced $W_{c,\infty}^{\alpha,\beta}$ based on this inequality as

$$W_{c,\infty}^{\alpha,\beta} = \alpha W_\infty^{\text{DFT}} + \beta E_x \tag{8}$$

so that α and β can be used as fitting parameters. This has been done to approximate the effect of $W_{1/2}$ on the MP AC without including it directly. For W_∞^{DFT} in eq 8, we use the accurate PC model approximation,[41,47,48]

$$W_\infty^{\text{DFT}}[\rho^{\text{HF}}] \approx \int\left[A\rho^{\text{HF}}(\mathbf{r})^{4/3} + B\frac{|\nabla\rho^{\text{HF}}(\mathbf{r})|^2}{\rho^{\text{HF}}(\mathbf{r})^{4/3}}\right]\mathrm{d}\mathbf{r} \tag{9}$$

where $A = -1.451$, $B = 5.317 \times 10^{-3}$. In our previous work, two new MP AC functionals,[30] SPL2 and MPACF-1, have been introduced. The SPL2 model for $W_{c,\lambda}$ reads

$$W_{c,\lambda}^{\text{SPL2}} = C_1 - \frac{m_1}{\sqrt{1+b_1\lambda}} - \frac{m_2}{\sqrt{1+b_2\lambda}} \tag{10}$$

with b_1, m_1, and C_1 fixed by the exact constraints: (i) $W_{c,\lambda}^{\text{SPL2}}$ vanishes at 0; (ii) its derivative at $\lambda = 0$ is equal to $2E_c^{\text{MP2}}$ (eq 4); and (iii) it converges to $W_{c,\infty}$ at $\lambda \rightarrow \infty$ (eq 5). The

https://doi.org/10.1021/acs.jpclett.3c01832
J. Phys. Chem. Lett. 2023, 14, 8448−8459

remaining parameters are fitted to the S22 set of NCIs.[49] MPACF1 (hereinafter F1) approximates E_c directly, resulting in

$$E_{c,\lambda}^{\mathrm{F1}} = -g\lambda + \frac{g(h+1)\lambda}{\sqrt{d_1^2\lambda + 1} + \sqrt[4]{d_2^4\lambda + 1}} \tag{11}$$

with g and h given in ref 30 and $E_{c,\lambda=1} = E_c$. In the original F1 formulation, α and β were set to 1 to reproduce the HEG correctly. However, here we use the general F1-form where $[d_1, d_2, \alpha, \beta]$ were fitted to the S22 data set. The advantage of F1 over SPL2 is that the former has the $\lambda^{-3/4}$ term in model $W_{c,\lambda\to\infty}$, which is missed by SPL2. Although the SPL2 and F1 functionals are not size-consistent by themselves, we recover size-consistency at no extra computational by applying the correction of ref 27.

Different MP2 Flavors Yield Different MP ACs. Here we consider the following general form for spin-scaled and regularized MP2[15] correlation energy:

$$E_c = c_{\mathrm{os}}E_c^{\kappa_{\mathrm{os}}\text{-MP2}} + c_{\mathrm{ss}}E_c^{\kappa_{\mathrm{ss}}\text{-MP2}} \tag{12}$$

with the opposite-spin (os) and the same-spin (ss) parts given by (closed-shell systems are assumed throughout this work)

$$E_c^{\kappa_{\mathrm{os}}\text{-MP2}} = -\sum_{abrs} \frac{\langle ab|rs\rangle^2}{\Delta_{ab}^{rs}}\left(1 - e^{-\kappa_{\mathrm{os}}\Delta_{ab}^{rs}}\right)^2 \tag{13}$$

and

$$E_c^{\kappa_{\mathrm{ss}}\text{-MP2}} = -\sum_{abrs} \frac{\langle ab|rs\rangle[\langle ab|rs\rangle - \langle rs|ba\rangle]}{\Delta_{ab}^{rs}}\left(1 - e^{-\kappa_{\mathrm{ss}}\Delta_{ab}^{rs}}\right)^2 \tag{14}$$

with $\Delta_{ab}^{rs} = \epsilon_r + \epsilon_s - \epsilon_a - \epsilon_b$ being an orbital gap between a pair of occupied (a and b) and a pair of virtual orbitals (r and s).

When the κ parameters are set to ∞, eq 12 reduces to the SCS-MP2 scheme,[17] with the two parameters c_{os} and c_{ss} (when these are further set to 1, eq 12 reduces to the standard MP2). The os part formally scales as N^4 whereas the ss part as N^5, where we refer to ref 18 for further clarifications and details on the scalings of SOS-MP2 vs SCS-MP2. Setting $c_{\mathrm{ss}} = 0$ defines the cheaper scaled opposite-spin-only (SOS) variant (with, e.g., $c_{\mathrm{os}} = 1.3$) .[18] When the κ parameters are set to a finite value, the divergence for vanishing gap is prevented. In general, similar regularization techniques are also employed in CASPT2[50] and Green's function methods.[51,52] For NCI, κ-MP2 provides significant improvements over MP2, particularly for values $\kappa \sim 1.2$.[15,53,54]

In the general expression of eq 12, we initially have four parameters that can be fitted. However, here we consider an OS variant with two parameters that require fitting, namely, c_{os} and κ_{os}, while c_{ss} is preset to 0. Our second MP2 variant has both ss and os spin channels but still two parameters to be fitted (κ_{ss} and κ_{os}) with c_{ss} and c_{os} preset to 1. To each of those, we can add the MP AC correction on top, yielding a large number of different functionals for the correlation energy. Here we focus on the three that are most promising (Table 1), and others can be found in Table S1 of the SI. For naming MP AC methods, we use the following notation: The string in front of the functional indicates which version of MP2 is used in that functional. So if regular MP2 is used within MP AC, the functional will just be called SPL2 or F1. If a modified version of MP2 has been used, such as c_{os}, κ_{os}-MP2, then the functional is called c_{os}, κ_{os}-SPL2 or c_{os}, κ_{os}-F1. Finally, $\kappa_{\mathrm{ss}}\kappa_{\mathrm{os}}$-SPL2 means that SPL2 interpolation has been used with the $\kappa_{\mathrm{ss}}\kappa_{\mathrm{os}}$-MP2 correlation energy (eq 12 with $c_{\mathrm{ss}} = c_{\mathrm{os}} = 1$).

Table 1. The Six Functionals that We Have Studied in This Work (in Addition to MP2 and SPL2) and the Parameters that Were Fitted to the S22 Data Set[a]

Method	c_{ss}	c_{os}	κ_{ss}	κ_{os}
MP2	1	1	∞	∞
SPL2	1	1	∞	∞
κ_{ss}, κ_{os}-MP2	1	1	0.9	1.4
κ_{ss}, κ_{os}-SPL2	1	1	1.1	1.7
κ-F1	1	1	1.5	1.5
$c_{\mathrm{os}}\kappa_{\mathrm{os}}$-MP2	0	2.1	0	0.9
$c_{\mathrm{os}}\kappa_{\mathrm{os}}$-SPL2	0	2.1	0	1.3
c_{os}-SPL2	0	1.8	∞	∞

[a]The parameters for other 14 combinations as well as the corresponding MP AC ones be found in Table S1 in the SI.

We acknowledge that employing a modified MP2 correlation energy as half of the initial slope of $W_{c,\lambda}$ deviates from the exact MP AC theory, which dictates the initial slope to be the unaltered MP2. Nevertheless, we adopt this pragmatic approach, recognizing the inherent flexibility of our MP AC construction, reflected in the end point of our MP AC curve, $W_{c,\infty}^{\alpha,\beta}$, which can adjust itself to the modified initial slope through the α and β parameters. Moreover, for larger NCI complexes, the radius of convergence of the MP series could be exceptionally small.[16,55] This could reduce the utility of the actual slope of the MP AC for approximating the true MP AC. Therefore, our approach, which involves regularization and scaling modifications of the initial MP AC slope, offers us a heuristic to capture MP ACs pertaining to NCIs. Simultaneously, this method provides an opportunity to decrease the computational cost of our MP AC construction, for instance, by using only the os part of MP2.

Returning to Table 1, we distinguish methods with computational scaling of N^5 (upper part of the table) from those with N^4 (lower part). We will compare the accuracy of these functionals with other common functionals B2PLYP-D3[10,56−61] (similar cost to our N^5 methods) and B3LYP-D3. Note that B3LYP-D3 has the same scaling as our N^4 methods but likely has a smaller prefactor. Nevertheless, SOS-MP2 can be implemented very efficiently[10,57−62]), with its wall times often being shorter than those for the HF calculation.[62]

Training of Our Functionals on S22. Similar to previous work,[30] we train the empirical parameters in our functional by minimizing their MAEs for the S22 data set.[49] Notice that for each κ value, the MP2 correlation energy needs to be recalculated, and we consider here κ-values between 0.6 and 1.7 with a 0.1 step. We also use c_{os} values from 1.0 to 2.5 with a step of 0.1. Note that the reoptimization of the MP AC parameters is needed any time an alteration to MP2 is made. Thus, for each combination of κ_{os} and κ_{ss} (or c_{os}), the corresponding parameters of the functionals are given in Table S2 in the SI.

In Figure 2, we show contour plots with the MAE for the S22 data set with the parameters of our selected methods (functionals). The two left-side panels display the S22 MAE contour plots for two distinct MP2 versions ($\kappa_{\mathrm{ss}}\kappa_{\mathrm{os}}$-MP2, an N^5 method; and $c_{\mathrm{os}}\kappa_{\mathrm{os}}$-MP2 an N^4 method) against their respective parameters. Conversely, the two right panels show the same plots after applying the SPL2 correction.

https://doi.org/10.1021/acs.jpclett.3c01832
J. Phys. Chem. Lett. 2023, 14, 8448−8459

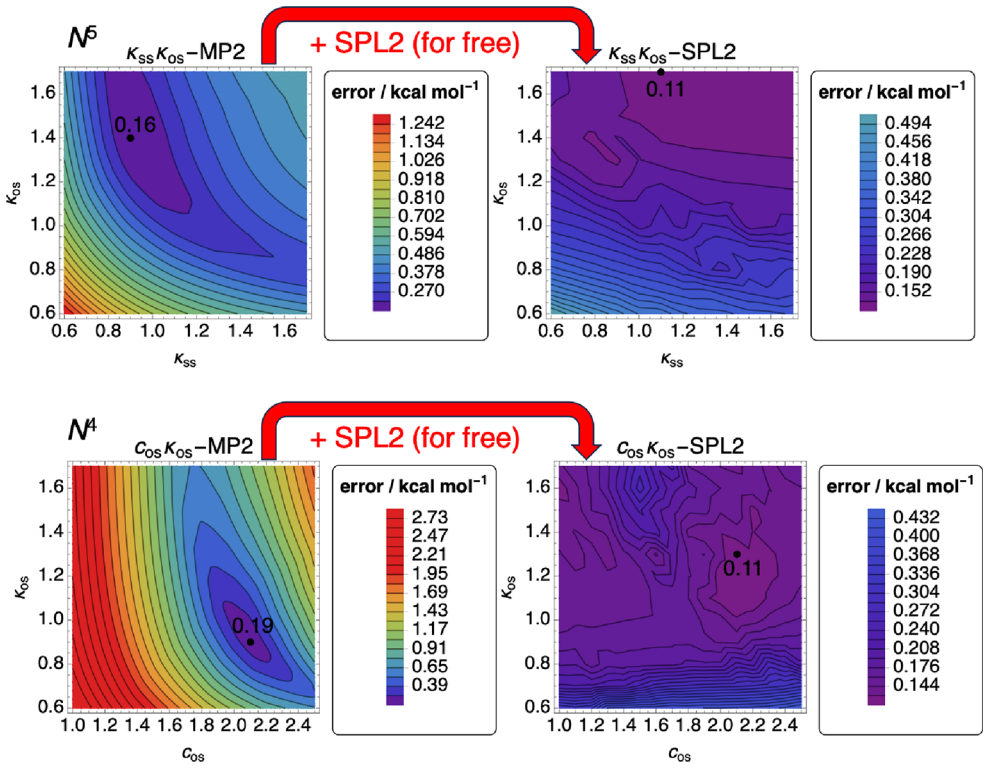

Figure 2. Top: The error between the interacting energy for the S22 data set between the CCSD(T) reference data and $\kappa_{ss}\kappa_{os}$-MP2 and $\kappa_{ss}\kappa_{os}$-SPL2 for a range of κ's between 0.6 and 1.7. Bottom: The same is true except for $c_{os}\kappa_{os}$-MP2 and $c_{os}\kappa_{os}$-SPL2 for a range of c_{os} values from 1 to 2.5 and κ_{os}'s between 0.6 and 1.7. The black dots denote the minimum energy of the contour plot with its corresponding value. A figure containing the curves of κ-MP2 and κ-SPL2, so the diagonals of the two top panels, can be found in the SI (figure S2).

Table 2. Total MAE's and Maximum Errors of the 5 NCI Data Sets Considered in This Work for the 8 Studied Functionals[a]

	S22		NCCE31		S66x8		X40		B30	
Method	MAE	MAX	MAE	MAX	MAE	MAX	MAE	MAX	MAE	MAX
MP2	0.86	3.47	0.5	2.53	0.39	4.15	0.34	2.39	0.86	3.73
SPL2	0.15	0.55	0.25	2.16	0.15	1.12	0.16	0.45	0.48	2.51
κ-F1	0.14	0.54	0.32	2.66	0.13	1.00	0.17	0.45	0.7	2.01
B2PLYP-D3	0.15[61]	0.71[61]	0.61[63]	2.41[63]	**0.11**[64]	0.90[64]	0.18	0.69	0.72	3.49
$c_{os}\kappa_{os}$-MP2	0.19	0.89	0.4	2.92	0.2	1.17	0.22	0.74	0.93	3.96
$c_{os}\kappa_{os}$-SPL2	**0.11**	**0.36**	0.27	2.23	**0.11**	**0.73**	**0.10**	**0.39**	**0.45**	**1.27**
c_{os}-SPL2	0.15	0.61	**0.21**	**1.84**	0.13	0.88	0.13	**0.39**	0.9	2.21
B3LYP-D3	0.31[61]	1.16[61]	0.60[63]	3.18[63]	0.15[64]	1.05[64]	0.22[65]	1.21[65]	1.36[65]	5.60[65]

[a]The best result for each column is highlighted in boldface. The S22 results for dRPA@PBE, RPA-SOSEX@PBE, and MP2C can be found in Table S3 from the SI. The NCCE31 results of dRPA@PBE can also be found in Table S4 of the SI. The box-plots of S22, NCCE31, B30, and X40 for MP2, B2PLYP-D3, $c_{os}\kappa_{os}$-SPL2, and B3LYP-D3 can be found in Figure S3, whereas the box-plots of S66x8 for the same functionals can be found in Figure S4.

Note that the SPL2 contour plots on the right are the result of reoptimizing the four SPL2 parameters (b_2, m_2, α, β) for each combination of the κ_{ss} and κ_{os} parameters (upper panel) and c_{os} and κ_{os} parameters (lower panel). The transition from the uncorrected MP2 versions (left panels) to the SPL2 corrected versions (right panels) yields a narrower range of MAEs, echoing our previous discussion on the adaptability of our MP AC construction to different MP2 inputs. The robustness of the SPL2 correction, regardless of the MP2 input, is further evidenced by the significant areas within both SPL2 contour plots that exhibit minimal MAE variation.

The top-left panel focuses on $\kappa_{ss}\kappa_{os}$-MP2 with regularizers κ_{ss} and κ_{os} as parameters. Here, the MAE is considerably more sensitive to the κ_{os} regularizer than to its same-spin counterpart. The minimum MAE is achieved at κ_{os} = 1.4 and κ_{ss} = 0.9 (0.16 kcal/mol). If we restrict $\kappa = \kappa_{ss} = \kappa_{os}$ as done in previous work,[15] the minimum is at κ = 1.1 with an MAE of 0.21 kcal/mol (see Figure S2 in the SI). Adding the SPL2 correction to $\kappa_{ss}\kappa_{os}$-MP2 (moving from the top-left to top-right panel) shifts the minimum to κ_{os} = 1.1 and κ_{ss} = 1.7, reducing it to 0.11 kcal/mol. While the reduction is modest, it is likely approaching the accuracy limit of MP2-like methods for the S22 data set. Importantly, we observe a relatively flat area around the minimum, suggesting that the MAE is almost constant as long as κ_{ss} and κ_{os} exceed approximately 1.1.

The lower-left panel illustrates the MAE for the opposite-spin-only $c_{os}\kappa_{os}$-MP2 with its parameters. Now the MAE depends substantially more on the c_{os} scaling factor than on the κ_{os} regularizer. The minimum is achieved at c_{os} = 2.1 and κ_{os} = 0.9, resulting in an MAE of 0.19 kcal/mol. This value is only

https://doi.org/10.1021/acs.jpclett.3c01832
J. Phys. Chem. Lett. 2023, 14, 8448−8459

marginally higher than the one from the upper panel, despite a significant reduction in computational cost. With the addition of the SPL2 correction to $c_{os}\kappa_{os}$-MP2 (transition from the lower-left to lower-right panel), the minimum MAE dips to 0.11 kcal/mol, slightly shifted to c_{os} = 2.1 and κ_{os} = 1.3. This MAE yields a significant improvement over $c_{os}\kappa_{os}$-MP2, and is on par with the more expensive $\kappa_{ss}\kappa_{os}$-SPL2 (top-right panel). Thus, through these explorations, we see the robustness of SPL2 in correcting various MP2 inputs.

$c_{os}\kappa_{os}$-MP2 as Our Workhorse. After training our functionals on S22, we test them on a variety of NCI data sets, with the results shown in Table 2. Alongside S22, we include NCCE31,[66−68] S66x8, X40, and B30. From Table 2, we can see that $c_{os}\kappa_{os}$-MP2 has the overall best performance (even when compared with more expensive N^5 methods).

In Figure 3, we use radar plots to show the performance of various functionals across five interaction-specific subsets in the NCCE31 data set, including hydrogen bonds (HB6), charge-transfer interactions (CT7), dipole interactions (DI6), weak interactions (WI7), and $\pi-\pi$-stacking interactions (PPS5). We can see that $c_{os}\kappa_{os}$-SPL2 exhibits superior performance in CT7, DI6, and PPS5 subsets, as well as the NCCE31 data set as a whole. While B2PLYP-D3 outperforms $c_{os}\kappa_{os}$-SPL2 for the WI7 subset, the differences in the MAEs are very small. In the HB6 subset, MP2 is the top performer, but the accuracy of $c_{os}\kappa_{os}$-SPL2 is still satisfactory and is similar to that of B2PLYP-D3.

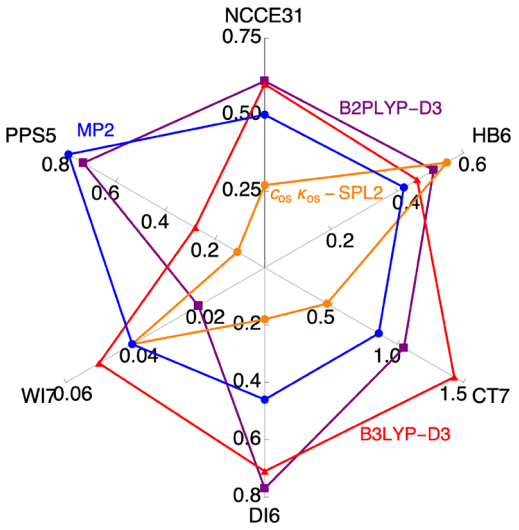

Figure 3. A radar plot for NCCE31 containing the MAEs in kcal/mol of the 5 subgroups (HB6, CT7, DI6, WI7, and PPS5) as well as the total MAE of MP2, $c_{os}\kappa_{os}$-SPL2, B3LYP-D3, and B2PLYP-D3. A table containing the MAEs of these methods as well as the other 4 methods studied in the paper can be found in the SI (Table S3). HB stands for hydrogen bonds, CT for charge transfer interaction, DI for dipole interactions, WI for weak interactions, and PPS for $\pi-\pi$-stacking interactions.

S66x8—Accuracy beyond Equilibrium. Turning our attention to the S66x8 data set,[64,70,71] we assess the performance of our functionals across NCIs beyond their geometric equilibrium (Table 3). We can see from the table that $c_{os}\kappa_{os}$-SPL2 (N^4 scaling) and B2PLYP-D3 (N^5 scaling) deliver twice the accuracy of MP2. For dispersion and mixed interactions, B3LYP-D3 shows a slightly better performance than our $c_{os}\kappa_{os}$-SPL2, but for the hydrogen-bonded complexes, B3LYP-D3 yields the poorest results.

From the box-plots shown in Figure 4, we observe the impact of SPL2 addition on the error distributions of MP2 and $c_{os}\kappa_{os}$-MP2 across individual categories within the S66x8 data set.

As expected,[30] SPL2 considerably improves "bare" MP2 across all categories. Using SPL2 to correct $c_{os}\kappa_{os}$-MP2 can be considered more challenging, as $c_{os}\kappa_{os}$-MP2 already gives significant improvements over MP2. Nevertheless, SPL2 also does a very good job here, as $c_{os}\kappa_{os}$-SPL2 surpasses $c_{os}\kappa_{os}$-MP2, both in terms of median values and the range of errors across all S66x8 categories. Moreover, as demonstrated in Figure 4, $c_{os}\kappa_{os}$-SPL2 (orange) significantly outperforms the original SPL2 (green), highlighting the dual advantage of our newly developed SPL2 formulation; it provides superior accuracy at a reduced computational cost.

Continuing with the S66x8 data set, Figure 5 shows dissociation curves for four S66 complexes: AcOH−Uracil (representing hydrogen bonds), Ethyne−Pyridine (mixed interactions), and Benzene−Ethene I and Pentane−Ethyne (both representing dispersion interactions). The dissociation curves of $c_{os}\kappa_{os}$-SPL2 align closely with those of the CCSD(T) reference. While B2PLYP-D3 also provides accurate curves, it is outperformed by $c_{os}\kappa_{os}$-SPL2 in the case of the mixed Ethyne−Pyridine complex. The $c_{os}\kappa_{os}$-SPL2 method effectively corrects the MP2 curves, both when MP2 underbinds (AcOH−Uracil), and when it overbinds (remaining complexes). In addition to errors in interaction energies, MP2 also displays significant errors in the equilibrium distances between dispersion-bonded fragments[72,73] (position of the minimum in

Table 3. Total MAEs and Maximum Errors of the S66x8 Data Set of 8 Functionals as well as the MAEs for Only the Hydrogen Bonding Complexes, the Dispersion Interaction Dominated Complexes, and the Mixed Set[a]I

	Total		H-bonds		Dispersion		Mixed	
Method	MAE	MAX	MAE	MAX	MAE	MAX	MAE	MAX
MP2	0.39	4.15	0.14	0.71	0.67	4.15	0.34	1.59
SPL2	0.15	1.12	0.12	0.42	0.21	1.12	0.1	0.75
κ-F1	0.13	1.00	0.09	0.44	0.19	1.00	0.11	0.60
B2PLYP-D3	**0.11**	0.90	0.09	**0.40**	0.14	0.90	**0.08**	0.52
$c_{os}\kappa_{os}$-MP2	0.2	1.17	0.14	1.00	0.32	1.17	0.14	0.64
$c_{os}\kappa_{os}$-SPL2	**0.11**	**0.73**	**0.08**	0.41	0.16	0.73	0.1	**0.48**
c_{os}-SPL2	0.13	0.88	0.11	0.58	0.16	0.88	0.1	0.53
B3LYP-D3	0.15	1.05	0.22	1.05	**0.13**	**0.65**	**0.08**	0.50

[a]The best result for each column is highlighted in boldface. The RPA-SOSEX(W, v_c)[69] results can be found in Table S5.

https://doi.org/10.1021/acs.jpclett.3c01832
J. Phys. Chem. Lett. 2023, 14, 8448−8459

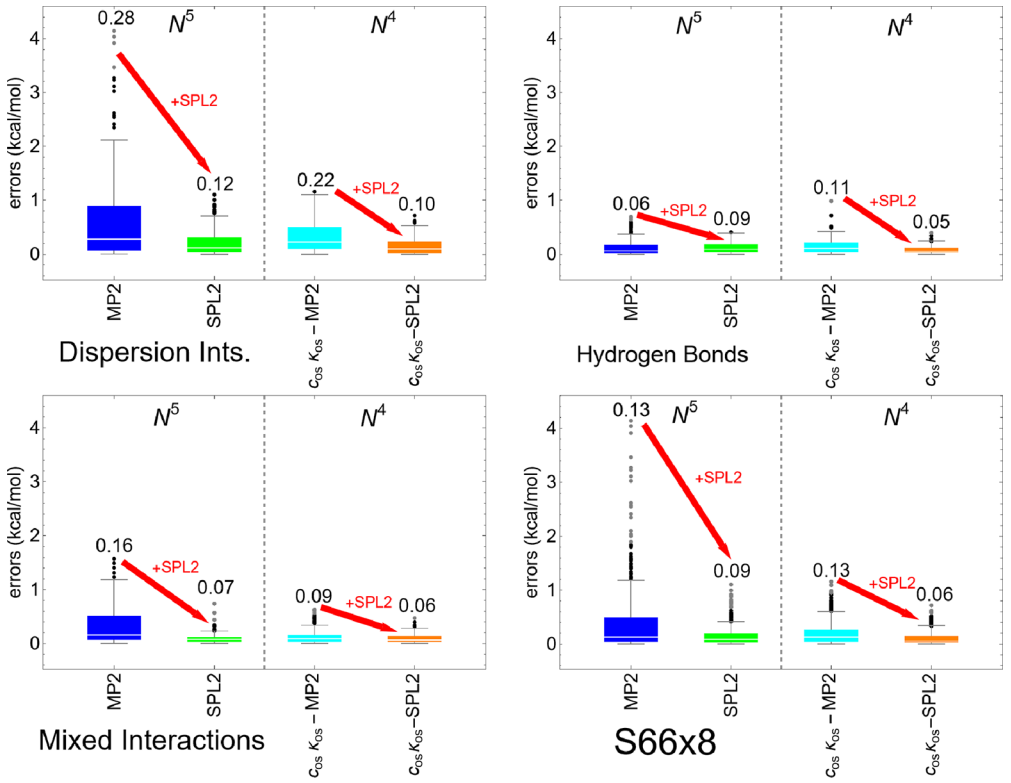

Figure 4. Box-plots including outliers as dots containing the errors of MP2, SPL2, and $c_{os}\kappa_{os}$-MP2 and $c_{os}\kappa_{os}$-MP2 for respectively the dispersion interactions (top left), hydrogen bonds (top right), mixed interactions (bottom left), and all interactions in total (bottom right), which show that the SPL2 form corrects the base MP2 form for the different kind of interactions of S66x8. Medians are denoted by a thin white line inside of each box, and the underlying median values are also given above each box. The box-plots of the remaining functionals can be found in Figure S5 in the SI. Box-plots showing how errors of different methods vary with the distances between fragments can be found in Figure S6 in the SI.

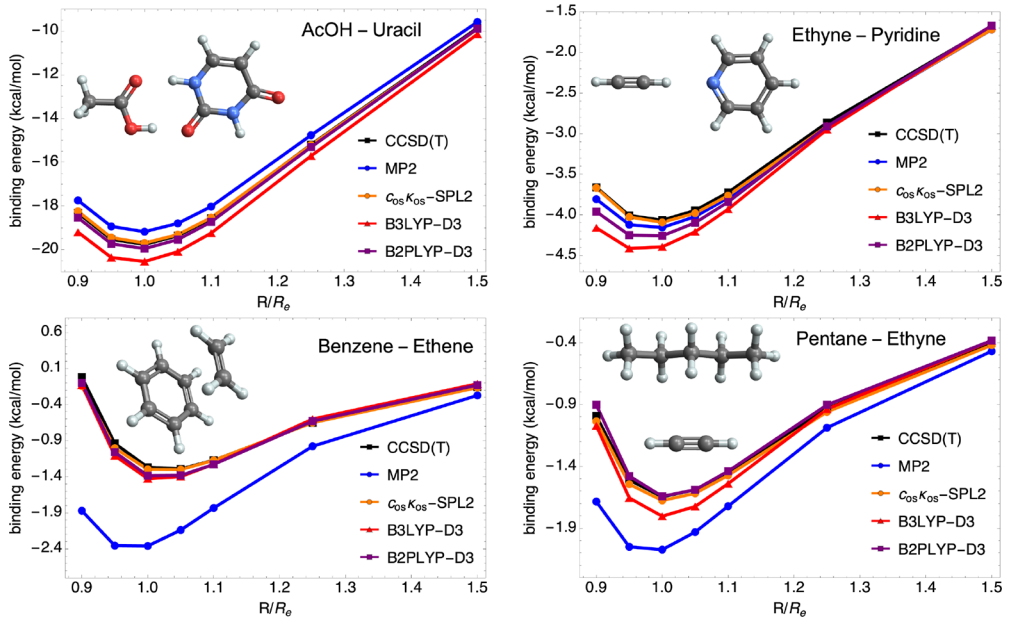

Figure 5. Dissociation curves of a dimer containing hydrogen bonds (top left) and containing mixed interactions (top right) and two dimers containing dispersion interactions (bottom) for conventional wave function methods (CCSD(T) and MP2), dispersion corrected DFT functionals (B3LYP-D3 and B2PLYP-D3), and our new $c_{os}\kappa_{os}$-SPL2 functional. The dissociation curves of all of the functionals can be found in the SI (Figure S7).

the dissociation curves), and this is also fixed by $c_{os}\kappa_{os}$-SPL2 (lower panels of Figure 5).

NCIs in Complexes Involving Halogens, Chalcogens, and Pnictogens. We extend our analysis to the NCI between molecules with halogen, chalcogen, and pnictogen atoms. Simulations of halogen bonds pose significant challenges to dispersion-corrected DFT, with difficulties often ascribed to the delocalization error inherent to density-functional approx-

https://doi.org/10.1021/acs.jpclett.3c01832
J. Phys. Chem. Lett. 2023, 14, 8448−8459

Table 4. Total MAEs and Maximum Errors of 31 Complexes from the X40 Data Set of 9 Functionals Split as well as the MAEs of the Separate Hydrogen Bonding, Halogen Bonding, and the Remaining NCIs[a]

	Total		H-bonds		HGB		Rest	
Method	MAE	MAX	MAE	MAX	MAE	MAX	MAE	MAX
MP2	0.34	2.39	0.26	1.08	0.27	0.87	0.48	2.39
SPL2	0.16	0.45	0.17	0.31	0.2	0.45	0.1	**0.18**
κ-F1	0.17	0.45	0.26	0.45	0.16	0.37	0.1	**0.18**
B2PLYP-D3	0.18	0.69	0.25	0.69	0.13	**0.18**	0.16	0.43
$c_{os}\kappa_{os}$-MP2	0.22	0.74	0.24	0.74	0.23	0.53	0.2	0.31
$c_{os}\kappa_{os}$-SPL2	**0.1**	**0.39**	**0.1**	**0.21**	0.12	0.27	**0.09**	0.39
c_{os}-SPL2	0.12	**0.39**	0.15	0.38	0.11	0.39	0.1	0.25
B3LYP-D3	0.22	1.21	0.46	1.21	**0.1**	0.20	0.13	0.31
M06-2X	0.27	0.90	0.24	0.40	0.40	0.90	0.17	0.35

[a]As in ref 65, we have removed the iodine complexes as they require relativistic corrections. This leaves the set with 31 different halogen bonded complexes, which have been also studied in the context of double hybrids[74,75] and the κ-regularizers.[15,20] The best result for each column is highlighted in boldface.

imations,[26,76−79] which cannot be fixed by empirical dispersion corrections such as D3 or D4.[26,76−79] However, accurately capturing halogen bonds is crucial, given their significant role in numerous biomolecular (protein−ligand) complexes and diverse crystalline materials.[35] We test our methods against the X40 data set from Řezáč et al.,[35] which includes a broad range of NCIs, spanning from hydrogen to pure halogen bonds in molecules containing halogens. Table 4 provides a summary of the results for the X40 data set, including the MAE for the overall X40 and for the hydrogen-bonded, halogen-bonded, and remaining complexes in the set. Once again, $c_{os}\kappa_{os}$-SPL2 is the most accurate method, outperforming MP2 by factors ranging from 2 to 5 depending on the X40 category. In comparison with B3LYP-D3, $c_{os}\kappa_{os}$-SPL2 exhibits comparable accuracy for halogen bonds and the "remaining" complexes, but surpasses B3LYP-D3 by a factor of 4.6 for hydrogen bonds. We have added M06-2X[80] to Table 4, a functional that was assessed reliable for halogen-bonded complexes.[77,81] Our results demonstrate that $c_{os}\kappa_{os}$-SPL2 significantly outperforms M06-2X, both for the entire X40 data set and for its subsets.

Before delving into more intricate halogen-bonded complexes, we note that $c_{os}\kappa_{os}$-SPL2 displays remarkably low errors for both S22 and X40. The two sets include NCIs of very different natures, and yet, $c_{os}\kappa_{os}$-SPL2 attains MAEs of 0.11 and 0.1 kcal/mol, respectively (approaching the uncertainties in the CCSD(T) reference itself[82]). This level of accuracy, unequaled among methods of similar or even higher computational cost, is highlighted in Figure 6. From this figure we can see that while κ-MP2.5[20] comes close to the performance of $c_{os}\kappa_{os}$-SPL2, it also comes at a higher computational cost (N^6 scaling).

The B30 data set, comprising halogen, chalcogen, and pnictogen bonds,[34] has proven to be an even more difficult challenge for DFT than X40,[65,74] being classified as a "difficult NCI" data set. In Table 5, the MAE of the full B30 set and the three separate subsets are displayed, and we can see that $c_{os}\kappa_{os}$-SPL2 outperforms other methods for halogen bonds (aHGB), with an MAE of 0.73 kcal/mol, significantly surpassing all competing methods. In the case of chalcogen bonds, however, $c_{os}\kappa_{os}$-SPL2 is surpassed by SPL2, and by MP2 for pnictogen bonds. Nevertheless, for the full B30 set, $c_{os}\kappa_{os}$-SPL2 is still a top performer.

The performance of $c_{os}\kappa_{os}$-SPL2 and the discrepancy in the accuracy of other methods for six B30 and eleven X40 halogen bonds are showcased in Figure 7. While the electron-donor in

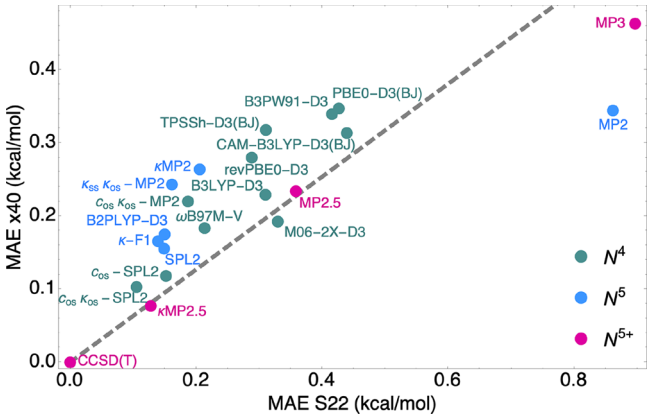

Figure 6. Correlation plot for the X40 and S22 MAE for methods with N^4, N^5, and N^{5+} scalings. The results for all the hybrid functionals were taken from ref 65, the results for B2PLYP-D3 for S22 were taken from ref 61 and for x40 were calculated using Turbomole (see Computational Details for more information), and the results for MP2.5, κMP2.5, and MP3 were taken from ref 20.

X40 is always a neutral species, in B30 it also can be an atomic anion. From Figure 7, we observe that both DFT-D3 and MP2 methods exhibit substantial errors for the more "extreme" B30 halogen-bond interactions. Yet, these methods demonstrate excellent performance for the remaining complexes, barring the MP2's performance for the last two, dominated by halogen−π interactions. For the B30 complexes in Figure 7, $c_{os}\kappa_{os}$-SPL2 is by far the most accurate, and its accuracy does not deteriorate once we move to the X40 complexes, suggesting that unlike other methods, $c_{os}\kappa_{os}$-SPL2 can accurately predict halogen interactions of different nature. The good performance of DFT-D3 for X40 halogen bonds and very bad for B30 is a consequence of large density-driven errors associated with the anions and charge-transfer prevalent in B30 halogen-bonded complexes. These errors have been extensively dissected in several studies.[26,76,83,84] Different RPA functionals with DFT orbitals struggle for the same reasons as the standard DFT functionals, with the density corrected variant of RPA giving improvements, albeit still performing worse (see Table S6 from the SI).[85]

Furthermore, in Figure 8, we show the dissociation curves of NH_3-FBr (complex 6 in Figure 7). Here, $c_{os}\kappa_{os}$-SPL2 again outperforms the other functionals and closely matches the CCSD(T) reference. Even though B3LYP-D3 and B2PLYP-D3

https://doi.org/10.1021/acs.jpclett.3c01832
J. Phys. Chem. Lett. 2023, 14, 8448−8459

Table 5. Total MAEs and Maximum Errors of the B30/Bauza30 Data Set of 9 Functionals Split as well as the MAEs of the Separate Halogen Bonding (Containing Mostly Anions as Donors), Chalcogen Bonding, and Pnictogen Bonding Complexes[a]

	Total		aHGB		CHB		PNB	
Method	MAE	MAX	MAE	MAX	MAE	MAX	MAE	MAX
MP2	0.86	3.73	2.22	3.73	0.63	1.21	**0.17**	**0.22**
SPL2	0.48	2.51	1.23	2.51	**0.2**	**0.66**	0.6	1.00
κ-F1	0.84	2.01	2.27	2.01	0.58	1.25	0.2	0.77
B2PLYP-D3	0.72	3.49	2.02	3.49	0.23	0.83	0.89	1.78
$c_{os}\kappa_{os}$-MP2	0.93	3.96	2.6	3.96	0.59	1.34	0.26	0.58
$c_{os}\kappa_{os}$-SPL2	**0.45**	**1.27**	**0.73**	**1.27**	0.4	0.92	0.31	0.61
c_{os}-SPL2	0.9	2.21	1.53	2.21	0.64	1.95	1.03	1.68
B3LYP-D3	1.36	5.60	3.50	5.60	0.98	2.10	0.36	0.91
M06-2X	0.99	3.22	1.80	3.22	0.59	1.80	1.36	1.71

[a]The best result for each column is highlighted in boldface. The MAEs and MAXs for 3 different RPA variants can be found in Table S6 in the SI.

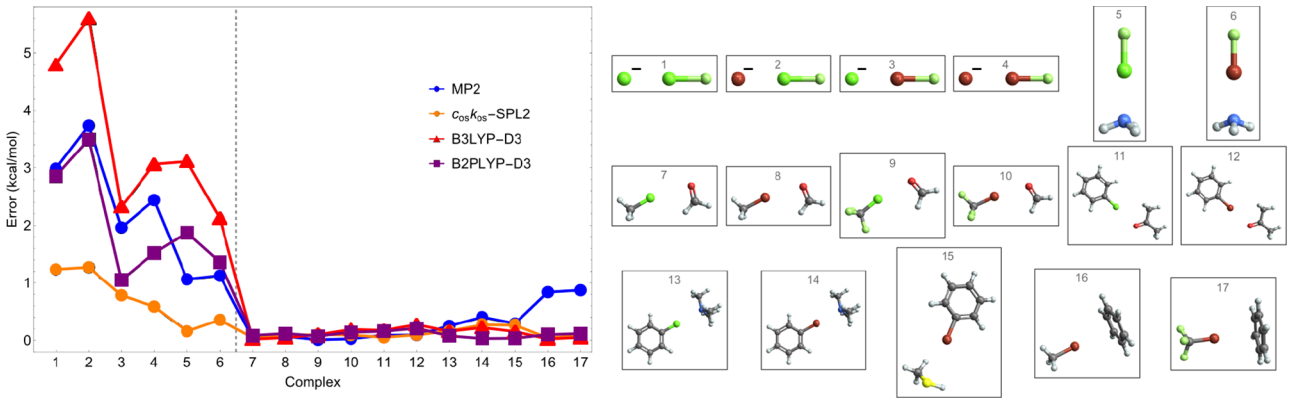

Figure 7. Errors between the CCSD(T) reference data[35,77] and MP2, c_{os}, κ_{os}-SPL2, B3LYP-D3, and B2PLYP-D3, respectively, for the halogen bonded complexes of the B30[34,77] and X40[35] data sets. The underlying complexes are shown on the right, with the first four containing negatively charged halogen atoms. The curves for $c_{os}\kappa_{os}$-MP2 and SPL2 can be found in the SI (left panel of Figure S8).

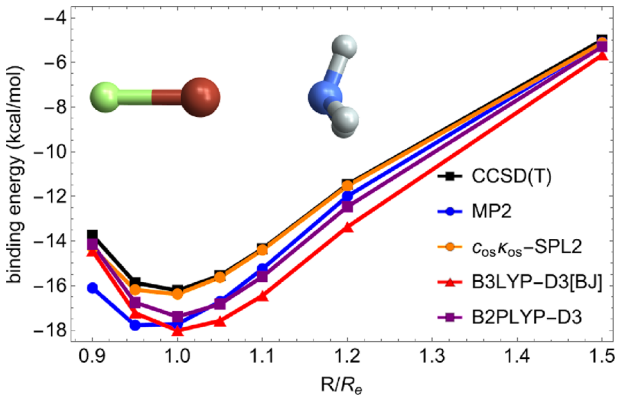

Figure 8. Dissociation curve of NH_3-FBr (complex 6) for CCSD(T), MP2, $c_{os}\kappa_{os}$-SPL2, B3LYP-D3[BJ], and B2PLYP-D3. Another dissociation curve of the B30 set can be found in the SI (right panel of Figure S8).

at small bond distances and MP2 at larger ones display good accuracy, $c_{os}\kappa_{os}$-SPL2 is the only method accurate around equilibrium. Similar conclusions can be drawn from the dissociation curve of another anionic halogen-bonded complex (see the right panel of Figure S8 in the SI).

In summary, $c_{os}\kappa_{os}$-SPL2 offers excellent performance for NCIs of various types. Building upon its SPL2 predecessor, $c_{os}\kappa_{os}$-SPL2 offers substantial improvements over both MP2 and dispersion-corrected (double) hybrid methods. Simultaneously, $c_{os}\kappa_{os}$-SPL2 achieves even greater accuracy than SPL2, while costing less (N^4 vs N^5 scaling). Further, we demonstrate the robustness and versatility of the SPL2 correction, showing its capability to significantly correct not only "bare" MP2, for which it was initially designed, but also various MP2 modifications. This flexibility is maintained while retaining, or even improving upon, the original SPL2 accuracy.

While we used a large aug-cc-pVQZ basis set in this study,[86] encouraged by SPL2's ability to absorb errors of both MP2 and its alterations, in the spirit of refs 87 and 88, we will also apply SPL2 to correct MP2 within smaller basis sets (e.g., that from ref 89). Finally, we will also use machine learning to create SPL2-like interpolations of the MP AC curve between its small and large λ limits. This approach could offer an even higher accuracy for NCIs.

COMPUTATIONAL DETAILS

For all calculations, PYSCF[90] is used to calculate the exchange energy, the HF density, and the MP2 correlation energy, which have been used for MP2 and SPL2 I& F1 forms. To calculate the κ-MP2 correlation energies, we used a python, PYSCF-like code with *numba* parallelization. This code and the full code for running MP AC calculations can be found in ref 91. Unless otherwise specified, we have used the aug-cc-pVQZ.[92] The exceptions are the bromide complexes of X40[35] for which we run Br with a aug-cc-pVQZ-pp basis set[93] and the corresponding pseudopotential[94] as done by Mardirossian et al.[65] A frozen core was also applied in these cases. The iodine complexes were removed from X40 due to the need for relativistic corrections.

https://doi.org/10.1021/acs.jpclett.3c01832
J. Phys. Chem. Lett. 2023, 14, 8448−8459

The reference data of S22 and S66x8 for B3LYP-D3 and B2PLYP-D3 can be found in refs 61 (def2-QZVP) and 64 (haVQZ), respectively. The NCCE31 data for both functionals are taken from ref 63 (aug-cc-pVTZ) for B3LYP-D3 and B2PLYP-D3. The B3LYP-D3 and M06-2X data for B30 are from refs 65 (aug-cc-pVTZ) and 20 (aug-cc-pVTZ), whereas the data for B2PLYP-D3 have been calculated using TURBOMOLE[95,96] with an aug-cc-pVQZ basis. For X40 the B3LYP-D3 and M06-2X data are from ref 65. (aug-cc-pVTZ) and the B2PLYP-D3 data have been calculated from the aug-cc-pVTZ basis set in TURBOMOLE. The data from the dissociation curves for MP2 and CCSD(T) have been also calculated with the same basis set with TURBOMOLE and extrapolated to the CBS limit. The B2PLYP-D3 and B3LYP-D3 dissociation curves have been calculated using a standard aug-cc-pVQZ basis set in TURBOMOLE, whereas the $c_{os}\kappa_{os}$-SPL2 has been run within the same basis set in PYSCF. For MP2C we have taken the reference data from ref 97 for S22 (extrapolated to the CBS limit). The dRPA data are obtained from ref 85 for S22 (cc-pVTZ) and B30 (cc-pVQZ) and from ref 98 for NCCE31 (ATZ). For RPA-SOSEX we got the data for S22 (cc-pVTZ) and B30 (cc-pVQZ) also from ref 85, but the S66x8 data (CBS limit) is from ref 69. Lastly the density corrected dRPA data, C(HF)-dRPA, were taken from ref 85. All of the RPA reference data were run using PBE orbitals. The fitted parameters of all the functionals, other than the ones from Table 1, can be found in Table S2 of the SI.

■ ASSOCIATED CONTENT

Data Availability Statement

The data that support the findings of this study are available within the main manuscript and its Supporting Information. Additional raw data and the code can also be found on Zenodo in ref 99 and ref 91. respectively.

Supporting Information

The Supporting Information is available free of charge at https://pubs.acs.org/doi/10.1021/acs.jpclett.3c01832.

Additional S66x8 plots, additional comparison data, parameters for the new methods, additional dissociation curves, and results for halogen bonds (PDF)

■ AUTHOR INFORMATION

Corresponding Author

Stefan Vuckovic − *Department of Chemistry, Faculty of Science and Medicine, Université de Fribourg/Universität Freiburg, CH-1700 Fribourg, Switzerland;* orcid.org/0000-0002-0768-9176; Email: stefan.vuckovic@unifr.ch

Authors

Kimberly J. Daas − *Department of Chemistry & Pharmaceutical Sciences and Amsterdam Institute of Molecular and Life Sciences (AIMMS), Faculty of Science, Vrije Universiteit, 1081HV Amsterdam, The Netherlands;* orcid.org/0000-0002-4323-6908

Derk P. Kooi − *Department of Chemistry & Pharmaceutical Sciences and Amsterdam Institute of Molecular and Life Sciences (AIMMS), Faculty of Science, Vrije Universiteit, 1081HV Amsterdam, The Netherlands; Microsoft Research AI4Science, 1118CZ Schiphol, The Netherlands;* orcid.org/0000-0001-9036-9722

Nina C. Peters − *Department of Chemistry & Pharmaceutical Sciences and Amsterdam Institute of Molecular and Life Sciences (AIMMS), Faculty of Science, Vrije Universiteit, 1081HV Amsterdam, The Netherlands*

Eduardo Fabiano − *Institute for Microelectronics and Microsystems (CNR-IMM), 73100 Lecce, Italy; Center for Biomolecular Nanotechnologies, Istituto Italiano di Tecnologia, 73010 Arnesano, Italy;* orcid.org/0000-0002-3990-669X

Fabio Della Sala − *Institute for Microelectronics and Microsystems (CNR-IMM), 73100 Lecce, Italy; Center for Biomolecular Nanotechnologies, Istituto Italiano di Tecnologia, 73010 Arnesano, Italy;* orcid.org/0000-0003-0940-8830

Paola Gori-Giorgi − *Department of Chemistry & Pharmaceutical Sciences and Amsterdam Institute of Molecular and Life Sciences (AIMMS), Faculty of Science, Vrije Universiteit, 1081HV Amsterdam, The Netherlands; Microsoft Research AI4Science, 1118CZ Schiphol, The Netherlands;* orcid.org/0000-0002-5952-1172

Complete contact information is available at: https://pubs.acs.org/10.1021/acs.jpclett.3c01832

Notes

The authors declare no competing financial interest.

■ ACKNOWLEDGMENTS

SV acknowledges funding from the SNSF Starting Grant project (TMSGI2_211246). KJD, DPK, and PG-G acknowledge financial support from The Netherlands Organisation for Scientific Research under Vici grant 724.017.001. FDS is grateful for the financial support from ICSC − Centro Nazionale di Ricerca in High Performance Computing, Big Data and Quantum Computing, funded by European Union − NextGenerationEU − PNRR. We want to thank Arno Förster for calculating the aug-QZ6P B2PLYP-D3 data for X40 and for fruitful discussions regarding this work. We also want to thank Suhwan Song for providing his MP2 data for the B30 data set and Lucas de Azevedo Santos and Klaas Giesbertz for insightful discussions.

■ REFERENCES

(1) Hohenstein, E. G.; Sherrill, C. D. Wavefunction methods for noncovalent interactions. *WIREs Computational Molecular Science* **2012**, *2*, 304−326.

(2) Riley, K. E.; Hobza, P. Noncovalent interactions in biochemistry. *WIREs Computational Molecular Science* **2011**, *1*, 3−17.

(3) Lao, K. U.; Herbert, J. M. Accurate and Efficient Quantum Chemistry Calculations for Noncovalent Interactions in Many-Body Systems: The XSAPT Family of Methods. *J. Phys. Chem. A* **2015**, *119*, 235−252.

(4) Sedlak, R.; Janowski, T.; Pitoňák, M.; Řezáč, J.; Pulay, P.; Hobza, P. Accuracy of Quantum Chemical Methods for Large Noncovalent Complexes. *J. Chem. Theory Comput.* **2013**, *9*, 3364−3374.

(5) Al-Hamdani, Y. S.; Tkatchenko, A. Understanding non-covalent interactions in larger molecular complexes from first principles. *J. Chem. Phys.* **2019**, *150*, 010901.

(6) Grimme, S.; Hansen, A.; Brandenburg, J. G.; Bannwarth, C. Dispersion-Corrected Mean-Field Electronic Structure Methods. *Chem. Rev.* **2016**, *116*, 5105−5154.

(7) Dubecký, M.; Mitas, L.; Jurečka, P. Noncovalent Interactions by Quantum Monte Carlo. *Chem. Rev.* **2016**, *116*, 5188−5215.

(8) Christensen, A. S.; Kubař, T.; Cui, Q.; Elstner, M. Semiempirical Quantum Mechanical Methods for Noncovalent Interactions for Chemical and Biochemical Applications. *Chem. Rev.* **2016**, *116*, 5301−5337.

(9) DiLabio, G. A.; Johnson, E. R.; Otero-de-la Roza, A. Performance of conventional and dispersion-corrected density-functional theory methods for hydrogen bonding interaction energies. *Phys. Chem. Chem. Phys.* **2013**, *15*, 12821−12828.
(10) Grimme, S.; Antony, J.; Ehrlich, S.; Krieg, H. A consistent and accurate ab initio parametrization of density functional dispersion correction (DFT-D) for the 94 elements H-Pu. *J. Chem. Phys.* **2010**, *132*, 154104.
(11) Hobza, P. The calculation of intermolecular interaction energies. *Annu. Rep. Prog. Chem., Sect. C: Phys. Chem.* **2011**, *107*, 148−168.
(12) Fabiano, E.; Constantin, L. A.; Della Sala, F. Wave Function and Density Functional Theory Studies of Dihydrogen Complexes. *J. Chem. Theory Comput.* **2014**, *10*, 3151−3162.
(13) Fabiano, E.; Cortona, P. Dispersion corrections applied to the TCA family of exchange-correlation functionals. *Theor. Chem. Acc.* **2017**, *136*, 88.
(14) Hobza, P.; Zahradnik, R. Intermolecular interactions between medium-sized systems. Nonempirical and empirical calculations of interaction energies. Successes and failures. *Chem. Rev.* **1988**, *88*, 871−897.
(15) Shee, J.; Loipersberger, M.; Rettig, A.; Lee, J.; Head-Gordon, M. Regularized Second-Order Møller−Plesset Theory: A More Accurate Alternative to Conventional MP2 for Noncovalent Interactions and Transition Metal Thermochemistry for the Same Computational Cost. *J. Phys. Chem. Lett.* **2021**, *12*, 12084−12097.
(16) Nguyen, B. D.; Chen, G. P.; Agee, M. M.; Burow, A. M.; Tang, M. P.; Furche, F. Divergence of Many-Body Perturbation Theory for Noncovalent Interactions of Large Molecules. *J. Chem. Theory Comput.* **2020**, *16*, 2258−2273.
(17) Grimme, S. Improved second-order Møller−Plesset perturbation theory by separate scaling of parallel- and antiparallel-spin pair correlation energies. *J. Chem. Phys.* **2003**, *118*, 9095−9102.
(18) Jung, Y.; Lochan, R. C.; Dutoi, A. D.; Head-Gordon, M. Scaled opposite-spin second order Møller−Plesset correlation energy: An economical electronic structure method. *J. Chem. Phys.* **2004**, *121*, 9793−9802.
(19) Lee, J.; Head-Gordon, M. Regularized Orbital-Optimized Second-Order Møller−Plesset Perturbation Theory: A Reliable Fifth-Order-Scaling Electron Correlation Model with Orbital Energy Dependent Regularizers. *J. Chem. Theory Comput.* **2018**, *14*, 5203−5219.
(20) Loipersberger, M.; Bertels, L. W.; Lee, J.; Head-Gordon, M. Exploring the Limits of Second- and Third-Order Møller−Plesset Perturbation Theories for Noncovalent Interactions: Revisiting MP2.5 and Assessing the Importance of Regularization and Reference Orbitals. *J. Chem. Theory Comput.* **2021**, *17*, 5582−5599.
(21) Grimme, S. Semiempirical hybrid density functional with perturbative second-order correlation. *J. Chem. Phys.* **2006**, *124*, 034108.
(22) Schwabe, T.; Grimme, S. Double-hybrid density functionals with long-range dispersion corrections: higher accuracy and extended applicability. *Phys. Chem. Chem. Phys.* **2007**, *9*, 3397−3406.
(23) Santra, G.; Sylvetsky, N.; Martin, J. M. L. Minimally Empirical Double-Hybrid Functionals Trained against the GMTKN55 Database: revDSD-PBEP86-D4, revDOD-PBE-D4, and DOD-SCAN-D4. *J. Phys. Chem. A* **2019**, *123*, 5129−5143.
(24) Zhang, Y.; Xu, X.; Goddard, W. A. Doubly hybrid density functional for accurate descriptions of nonbond interactions, thermochemistry, and thermochemical kinetics. *Proc. Natl. Acad. Sci. U. S. A.* **2009**, *106*, 4963−4968.
(25) Zhang, I. Y.; Xu, X. Exploring the Limits of the XYG3-Type Doubly Hybrid Approximations for the Main-Group Chemistry: The xDH@B3LYP Model. *J. Phys. Chem. Lett.* **2021**, *12*, 2638−2644.
(26) Song, S.; Vuckovic, S.; Sim, E.; Burke, K. Density Sensitivity of Empirical Functionals. *J. Phys. Chem. Lett.* **2021**, *12*, 800−807.
(27) Vuckovic, S.; Gori-Giorgi, P.; Della Sala, F.; Fabiano, E. Restoring size consistency of approximate functionals constructed from the adiabatic connection. *J. Phys. Chem. Lett.* **2018**, *9*, 3137−3142.
(28) Caldeweyher, E.; Ehlert, S.; Hansen, A.; Neugebauer, H.; Spicher, S.; Bannwarth, C.; Grimme, S. A generally applicable atomic-charge dependent London dispersion correction. *J. Chem. Phys.* **2019**, *150*, 154122.
(29) Caldeweyher, E.; Mewes, J.-M.; Ehlert, S.; Grimme, S. Extension and evaluation of the D4 London-dispersion model for periodic systems. *Phys. Chem. Chem. Phys.* **2020**, *22*, 8499−8512.
(30) Daas, T. J.; Fabiano, E.; Della Sala, F.; Gori-Giorgi, P.; Vuckovic, S. Noncovalent Interactions from Models for the Møller−Plesset Adiabatic Connection. *J. Phys. Chem. Lett.* **2021**, *12*, 4867−4875.
(31) Giarrusso, S.; Gori-Giorgi, P.; Della Sala, F.; Fabiano, E. Assessment of interaction-strength interpolation formulas for gold and silver clusters. *J. Chem. Phys.* **2018**, *148*, 134106.
(32) Daas, T. J.; Grossi, J.; Vuckovic, S.; Musslimani, Z. H.; Kooi, D. P.; Seidl, M.; Giesbertz, K. J. H.; Gori-Giorgi, P. Large coupling-strength expansion of the Møller−Plesset adiabatic connection: From paradigmatic cases to variational expressions for the leading terms. *J. Chem. Phys.* **2020**, *153*, 214112.
(33) Vuckovic, S.; Fabiano, E.; Gori-Giorgi, P.; Burke, K. MAP: An MP2 Accuracy Predictor for Weak Interactions from Adiabatic Connection Theory. *J. Chem. Theory Comput.* **2020**, *16*, 4141−4149.
(34) Bauzá, A.; Alkorta, I.; Frontera, A.; Elguero, J. On the Reliability of Pure and Hybrid DFT Methods for the Evaluation of Halogen, Chalcogen, and Pnicogen Bonds Involving Anionic and Neutral Electron Donors. *J. Chem. Theory Comput.* **2013**, *9*, 5201−5210.
(35) Řezáč, J.; Riley, K. E.; Hobza, P. Benchmark Calculations of Noncovalent Interactions of Halogenated Molecules. *J. Chem. Theory Comput.* **2012**, *8*, 4285−4292.
(36) Seidl, M.; Perdew, J. P.; Levy, M. Strictly correlated electrons in density-functional theory. *Phys. Rev. A* **1999**, *59*, 51−54.
(37) Pernal, K. Correlation energy from random phase approximations: A reduced density matrices perspective. *Int. J. Quantum Chem.* **2018**, *118*, No. e25462.
(38) Seidl, M.; Giarrusso, S.; Vuckovic, S.; Fabiano, E.; Gori-Giorgi, P. Communication: Strong-interaction limit of an adiabatic connection in Hartree-Fock theory. *J. Chem. Phys.* **2018**, *149*, 241101.
(39) Daas, T. J.; Kooi, D. P.; Grooteman, A. J. A. F.; Seidl, M.; Gori-Giorgi, P. Gradient Expansions for the Large-Coupling Strength Limit of the Møller−Plesset Adiabatic Connection. *J. Chem. Theory Comput.* **2022**, *18*, 1584−1594.
(40) Burton, H. G. A.; Marut, C.; Daas, T. J.; Gori-Giorgi, P.; Loos, P.-F. Variations of the Hartree−Fock fractional-spin error for one electron. *J. Chem. Phys.* **2021**, *155*, 054107.
(41) Seidl, M.; Gori-Giorgi, P.; Savin, A. Strictly correlated electrons in density-functional theory: A general formulation with applications to spherical densities. *Phys. Rev. A* **2007**, *75*, 042511.
(42) Gori-Giorgi, P.; Vignale, G.; Seidl, M. Electronic Zero-Point Oscillations in the Strong-Interaction Limit of Density Functional Theory. *J. Chem. Theory Comput.* **2009**, *5*, 743−753.
(43) Gori-Giorgi, P.; Seidl, M.; Savin, A. Intracule densities in the strong-interaction limit of density functional theory. *Phys. Chem. Chem. Phys.* **2008**, *10*, 3440−3446.
(44) Gori-Giorgi, P.; Seidl, M.; Vignale, G. Density-Functional Theory for Strongly Interacting Electrons. *Phys. Rev. Lett.* **2009**, *103*, 166402.
(45) Grossi, J.; Kooi, D. P.; Giesbertz, K. J. H.; Seidl, M.; Cohen, A. J.; Mori-Sánchez, P.; Gori-Giorgi, P. Fermionic statistics in the strongly correlated limit of Density Functional Theory. *J. Chem. Theory Comput.* **2017**, *13*, 6089−6100.
(46) Vuckovic, S.; Gerolin, A.; Daas, T. J.; Bahmann, H.; Friesecke, G.; Gori-Giorgi, P. Density functionals based on the mathematical structure of the strong-interaction limit of DFT. *WIREs Computational Molecular Science* **2023**, e1634.
(47) Seidl, M.; Perdew, J. P.; Kurth, S. Density functionals for the strong-interaction limit. *Phys. Rev. A* **2000**, *62*, 012502.

https://doi.org/10.1021/acs.jpclett.3c01832
J. Phys. Chem. Lett. 2023, 14, 8448−8459

(48) Mirtschink, A.; Seidl, M.; Gori-Giorgi, P. Energy densities in the strong-interaction limit of density functional theory. *J. Chem. Theory Comput.* **2012**, *8*, 3097−3107.
(49) Jurečka, P.; Šponer, J.; Černý, J.; Hobza, P. Benchmark database of accurate (MP2 and CCSD(T) complete basis set limit) interaction energies of small model complexes, DNA base pairs, and amino acid pairs. *Phys. Chem. Chem. Phys.* **2006**, *8*, 1985−1993.
(50) Battaglia, S.; Fransén, L.; Fdez. Galván, I.; Lindh, R. Regularized CASPT2: an Intruder-State-Free Approach. *J. Chem. Theory Comput.* **2022**, *18*, 4814−4825.
(51) Monino, E.; Loos, P.-F. Unphysical discontinuities, intruder states and regularization in GW methods. *J. Chem. Phys.* **2022**, *156*, 231101.
(52) Marie, A.; Loos, P.-F. A Similarity Renormalization Group Approach to Green's Function Methods. *J. Chem. Theory Comput.* **2023**, *19*, 3943−3957.
(53) Rettig, A.; Shee, J.; Lee, J.; Head-Gordon, M. Revisiting the Orbital Energy-Dependent Regularization of Orbital-Optimized Second-Order Møller−Plesset Theory. *J. Chem. Theory Comput.* **2022**, *18*, 5382−5392.
(54) Santra, G.; Martin, J. M. L. Do Double-Hybrid Functionals Benefit from Regularization in the PT2 Term? Observations from an Extensive Benchmark. *J. Phys. Chem. Lett.* **2022**, *13*, 3499−3506.
(55) Nguyen, B. D.; Hernandez, D. J.; Flores, E. V.; Furche, F. Dispersion size-consistency. *Electronic Structure* **2022**, *4*, 014003.
(56) Grimme, S. Semiempirical GGA-type density functional constructed with a long-range dispersion correction. *J. Comput. Chem.* **2006**, *27*, 1787−1799.
(57) Elstner, M.; Hobza, P.; Frauenheim, T.; Suhai, S.; Kaxiras, E. Hydrogen bonding and stacking interactions of nucleic acid base pairs: A density-functional-theory based treatment. *J. Chem. Phys.* **2001**, *114*, 5149−5155.
(58) Wu, Q.; Yang, W. Empirical correction to density functional theory for van der Waals interactions. *J. Chem. Phys.* **2002**, *116*, 515−524.
(59) Grimme, S. Accurate description of van der Waals complexes by density functional theory including empirical corrections. *J. Comput. Chem.* **2004**, *25*, 1463−1473.
(60) Becke, A. D.; Johnson, E. R. A unified density-functional treatment of dynamical, nondynamical, and dispersion correlations. *J. Chem. Phys.* **2007**, *127*, 124108.
(61) Goerigk, L.; Hansen, A.; Bauer, C.; Ehrlich, S.; Najibi, A.; Grimme, S. A look at the density functional theory zoo with the advanced GMTKN55 database for general main group thermochemistry, kinetics and noncovalent interactions. *Phys. Chem. Chem. Phys.* **2017**, *19*, 32184−32215.
(62) Förster, A.; Franchini, M.; van Lenthe, E.; Visscher, L. A Quadratic Pair Atomic Resolution of the Identity Based SOS-AO-MP2 Algorithm Using Slater Type Orbitals. *J. Chem. Theory Comput.* **2020**, *16*, 875−891.
(63) Liakos, D. G.; Neese, F. Is It Possible To Obtain Coupled Cluster Quality Energies at near Density Functional Theory Cost? Domain-Based Local Pair Natural Orbital Coupled Cluster vs Modern Density Functional Theory. *J. Chem. Theory Comput.* **2015**, *11*, 4054−4063.
(64) Brauer, B.; Kesharwani, M. K.; Kozuch, S.; Martin, J. M. L. The S66x8 benchmark for noncovalent interactions revisited: explicitly correlated ab initio methods and density functional theory. *Phys. Chem. Chem. Phys.* **2016**, *18*, 20905−20925.
(65) Mardirossian, N.; Head-Gordon, M. Thirty years of density functional theory in computational chemistry: an overview and extensive assessment of density functionals. *Mol. Phys.* **2017**, *115*, 2315−2372.
(66) Zhao, Y.; Truhlar, D. G. Design of Density Functionals That Are Broadly Accurate for Thermochemistry, Thermochemical Kinetics, and Nonbonded Interactions. *J. Phys. Chem. A* **2005**, *109*, 5656−5667.
(67) Zhang, I. Y.; Xu, X.; Jung, Y.; Goddard, W. A. A fast doubly hybrid density functional method close to chemical accuracy using a local opposite spin ansatz. *Proc. Natl. Acad. Sci. U. S. A.* **2011**, *108*, 19896−19900.
(68) Peverati, R.; Truhlar, D. G. Quest for a universal density functional: the accuracy of density functionals across a broad spectrum of databases in chemistry and physics. *Philos. Trans. R. Soc. A* **2014**, *372*, 20120476.
(69) Förster, A. Assessment of the Second-Order Statically Screened Exchange Correction to the Random Phase Approximation for Correlation Energies. *J. Chem. Theory Comput.* **2022**, *18*, 5948−5965.
(70) Řezáč, J.; Riley, K. E.; Hobza, P. S66: A Well-balanced Database of Benchmark Interaction Energies Relevant to Biomolecular Structures. *J. Chem. Theory Comput.* **2011**, *7*, 2427−2438.
(71) Santra, G.; Semidalas, E.; Mehta, N.; Karton, A.; Martin, J. M. L. S66x8 noncovalent interactions revisited: new benchmark and performance of composite localized coupled-cluster methods. *Phys. Chem. Chem. Phys.* **2022**, *24*, 25555−25570.
(72) Vuckovic, S.; Burke, K. Quantifying and Understanding Errors in Molecular Geometries. *J. Phys. Chem. Lett.* **2020**, *11*, 9957−9964.
(73) Vuckovic, S. Quantification of Geometric Errors Made Simple: Application to Main-Group Molecular Structures. *J. Phys. Chem. A* **2022**, *126*, 1300−1311.
(74) Mardirossian, N.; Head-Gordon, M. Survival of the most transferable at the top of Jacob's ladder: Defining and testing the ωB97M(2) double hybrid density functional. *J. Chem. Phys.* **2018**, *148*, 241736.
(75) Förster, A.; Visscher, L. Double hybrid DFT calculations with Slater type orbitals. *J. Comput. Chem.* **2020**, *41*, 1660−1684.
(76) Kim, Y.; Song, S.; Sim, E.; Burke, K. Halogen and Chalcogen Binding Dominated by Density-Driven Errors. *J. Phys. Chem. Lett.* **2019**, *10*, 295−301.
(77) Otero-de-la Roza, A.; Johnson, E. R.; DiLabio, G. A. Halogen Bonding from Dispersion-Corrected Density-Functional Theory: The Role of Delocalization Error. *J. Chem. Theory Comput.* **2014**, *10*, 5436−5447.
(78) Song, S.; Vuckovic, S.; Kim, Y.; Yu, H.; Sim, E.; Burke, K. Extending density functional theory with near chemical accuracy beyond pure water. *Nat. Commun.* **2023**, *14*, 14.
(79) Mehta, N.; Fellowes, T.; White, J. M.; Goerigk, L. CHAL336 Benchmark Set: How Well Do Quantum-Chemical Methods Describe Chalcogen-Bonding Interactions? *J. Chem. Theory Comput.* **2021**, *17*, 2783−2806.
(80) Zhao, Y.; Truhlar, D. The M06 suite of density functionals for main group thermochemistry, thermochemical kinetics, noncovalent interactions, excited states, and transition elements: two new functionals and systematic testing of four M06-class functionals and 12 other functionals. *Theor. Chem. Acc.* **2008**, *120*, 215.
(81) de Azevedo Santos, L.; Ramalho, T. C.; Hamlin, T. A.; Bickelhaupt, F. M. Chalcogen bonds: Hierarchical ab initio benchmark and density functional theory performance study. *J. Comput. Chem.* **2021**, *42*, 688−698.
(82) Řezáč, J.; Dubecký, M.; Jurečka, P.; Hobza, P. Extensions and applications of the A24 data set of accurate interaction energies. *Phys. Chem. Chem. Phys.* **2015**, *17*, 19268−19277.
(83) Sim, E.; Song, S.; Vuckovic, S.; Burke, K. Improving Results by Improving Densities: Density-Corrected Density Functional Theory. *J. Am. Chem. Soc.* **2022**, *144*, 6625−6639.
(84) Song, S.; Vuckovic, S.; Sim, E.; Burke, K. Density-Corrected DFT Explained: Questions and Answers. *J. Chem. Theory Comput.* **2022**, *18*, 817−827.
(85) Graf, D.; Thom, A. J. W. Corrected Density Functional Theory and the Random Phase Approximation: Improved Accuracy at Little Extra Cost. *arXiv*, 2307.00389, 2023.
(86) Fabiano, E.; Gori-Giorgi, P.; Seidl, M.; Della Sala, F. Interaction-Strength Interpolation Method for Main-Group Chemistry: Benchmarking, Limitations, and Perspectives. *J. Chem. Theory. Comput.* **2016**, *12*, 4885−4896.
(87) Giner, E.; Pradines, B.; Ferté, A.; Assaraf, R.; Savin, A.; Toulouse, J. Curing basis-set convergence of wave-function theory

https://doi.org/10.1021/acs.jpclett.3c01832
J. Phys. Chem. Lett. 2023, 14, 8448−8459

using density-functional theory: A systematically improvable approach. *J. Chem. Phys.* **2018**, *149*, 194301.
(88) Traore, D.; Giner, E.; Toulouse, J. Basis-set correction based on density-functional theory: Rigorous framework for a one-dimensional model. *J. Chem. Phys.* **2022**, *156*, 044113.
(89) Mehta, N.; Martin, J. M. L. MP2-F12 Basis Set Convergence near the Complete Basis Set Limit: Are h Functions Sufficient? *J. Phys. Chem. A* **2022**, *126*, 3964−3971.
(90) Sun, Q.; Berkelbach, T. C.; Blunt, N. S.; Booth, G. H.; Guo, S.; Li, Z.; Liu, J.; McClain, J. D.; Sayfutyarova, E. R.; Sharma, S.; et al. PySCF: the Python-based simulations of chemistry framework. *Wiley Interdiscip. Rev.: Comput. Mol. Sci.* **2018**, *8*, No. e1340.
(91) Daas, K. J., Kooi, D. P., Vuckovic, S. *tjdaas/kappa-SPL2: kappa-SPL2 v.1.0.5*. 2023. https://zenodo.org/record/8224499.
(92) Dunning, T. H. Gaussian basis sets for use in correlated molecular calculations. I. The atoms boron through neon and hydrogen. *J. Chem. Phys.* **1989**, *90*, 1007−1023.
(93) Peterson, K. A.; Figgen, D.; Goll, E.; Stoll, H.; Dolg, M. Systematically convergent basis sets with relativistic pseudopotentials. II. Small-core pseudopotentials and correlation consistent basis sets for the post 16−18 elements. *J. Chem. Phys.* **2003**, *119*, 11113−11123.
(94) Kozuch, S.; Martin, J. M. L. Halogen Bonds: Benchmarks and Theoretical Analysis. *J. Chem. Theory Comput.* **2013**, *9*, 1918−1931.
(95) *TURBOMOLE*, V7.1 2010, a development of University of Karlsruhe and Forschungszentrum Karlsruhe GmbH, 1989−2007; TURBOMOLE GmbH, since 2007; available from http://www.turbomole.com.
(96) Furche, F.; Ahlrichs, R.; Hättig, C.; Klopper, W.; Sierka, M.; Weigend, F. Turbomole. *WIREs Computational Molecular Science* **2014**, *4*, 91−100.
(97) Pitoňák, M.; Heßelmann, A. Accurate Intermolecular Interaction Energies from a Combination of MP2 and TDDFT Response Theory. *J. Chem. Theory Comput.* **2010**, *6*, 168−178.
(98) Mezei, P. D.; Csonka, G. I.; Ruzsinszky, A.; Kállay, M. Construction and Application of a New Dual-Hybrid Random Phase Approximation. *J. Chem. Theory Comput.* **2015**, *11*, 4615−4626.
(99) Daas, K. J.; Kooi, D. P.; Peters, N. C.; Fabiano, E.; Della Sala, F.; Gori-Giorgi, P.; Vuckovic, S. *Data: Regularized and Opposite spin-scaled functionals from Møller-Plesset adiabatic connection − higher accuracy at lower cost (arXiv.2307.02715)*. 2023. https://zenodo.org/record/8118099.

https://doi.org/10.1021/acs.jpclett.3c01832
J. Phys. Chem. Lett. 2023, 14, 8448−8459